TU Delft

Delft University of Technology

Effect of drag reducing riblet surface on coherent structure in turbulent boundary layer

CUI, Guangyao; PAN, C.; WU, Di; YE, Qingqing; WANG, Jinjun

DOI
10.1016/j.cja.2019.04.023

Publication date
2019

Document Version
Final published version

Published in
Chinese Journal of Aeronautics

Citation (APA)
CUI, G., PAN, C., WU, D., YE, Q., & WANG, J. (2019). Effect of drag reducing riblet surface on coherent structure in turbulent boundary layer. *Chinese Journal of Aeronautics*, *32*(11), 2433-2442. https://doi.org/10.1016/j.cja.2019.04.023

Important note
To cite this publication, please use the final published version (if applicable).
Please check the document version above.

Copyright
Other than for strictly personal use, it is not permitted to download, forward or distribute the text or part of it, without the consent of the author(s) and/or copyright holder(s), unless the work is under an open content license such as Creative Commons.

Takedown policy
Please contact us and provide details if you believe this document breaches copyrights.
We will remove access to the work immediately and investigate your claim.

This work is downloaded from Delft University of Technology.
For technical reasons the number of authors shown on this cover page is limited to a maximum of 10.

Chinese Journal of Aeronautics, (2019), 32(11): 2433–2442

Chinese Society of Aeronautics and Astronautics
& Beihang University

Chinese Journal of Aeronautics

cja@buaa.edu.cn
www.sciencedirect.com

Effect of drag reducing riblet surface on coherent structure in turbulent boundary layer

Guangyao CUI [a], Chong PAN [a], Di WU [a], Qingqing YE [b,*], Jinjun WANG [a]

[a] School of Aeronautical Science and Engineeting, Beihang University, Beijing 100083, China
[b] Department of Aerodynamics, Wind Energy, Flight Performance & Propulsion, Delft University of Technology, NL-2629 HS Delft, Netherlands

Received 17 September 2018; revised 9 October 2018; accepted 2 January 2019
Available online 30 May 2019

KEYWORDS

Coherent structures;
Particle image velocimetry;
Riblet;
Riblet surface;
Turbulent boundary layer;
Uniform momentum zones

Abstract The characteristics of turbulent boundary layer over streamwise aligned drag reducing riblet surface under zero-pressure gradient are investigated using particle image velocimetry. The formation and distribution of large-scale coherent structures and their effect on momentum partition are analyzed using two-point correlation and probability density function. Compared with smooth surface, the streamwise riblets reduce the friction velocity and Reynolds stress in the turbulent boundary layer, indicating the drag reduction effect. Strong correlation has been found between the occurrence of hairpin vortices and the momentum distribution. The number and streamwise length scale of hairpin vortices decrease over streamwise riblet surface. The correlation between number of uniform momentum zones and Reynolds number remains the same as smooth surface.
© 2019 Chinese Society of Aeronautics and Astronautics. Production and hosting by Elsevier Ltd. This is an open access article under the CC BY-NC-ND license (http://creativecommons.org/licenses/by-nc-nd/4.0/).

1. Introduction

The existence of multi-scale, randomly distributed coherent structures is well-known in the studies of the dynamic behavior of turbulent boundary layer. Hairpin vortex packets are the dominant coherent structures developing in the turbulent boundary layer.[1–6] The hairpin vortices are widely distributed along the streamwise direction, inducing strong ejection (Q2) and sweep (Q4) events and high-level shear stress ($-\langle u'v'\rangle$).[7] Robinson[8] reviewed that vortex structures of various forms are widely distributed in the outer region. Adrian et al.[1] pointed out that hairpin-shaped vortices occur in streamwise-aligned packets which propagate with small velocity dispersion in the outer region. Furthermore, Adrian[2] concluded that the hairpins are most common in the logarithmic layer and become less frequent with wall-normal height, occasionally penetrating across the entire turbulent boundary layer. Furthermore, Lee and Li[9] applied hydrogen bubble visualization and two-dimensional hot film measurement to investigate the soliton-like coherent structures and hairpin vortices, indicating that these coherent structures are dominant in almost all dynamic processes in both the early and later stages of boundary-layer transitions as well as in a turbulent boundary layer. By using two-dimensional Particle Image Velocimetry (PIV), Natrajan et al.[10] suggested that the three-dimensional hairpin vortices appear as pairs of counter-rotating spanwise

* Corresponding author.
E-mail address: Q.Ye-1@tudelft.nl (Q. YE).
Peer review under responsibility of Editorial Committee of CJA.

Production and hosting by Elsevier

https://doi.org/10.1016/j.cja.2019.04.023
1000-9361 © 2019 Chinese Society of Aeronautics and Astronautics. Production and hosting by Elsevier Ltd.
This is an open access article under the CC BY-NC-ND license (http://creativecommons.org/licenses/by-nc-nd/4.0/).

vortices in the streamwise-wall-normal cross-section. The clockwise and counterclockwise rotating spanwise vortices (also referred to as prograde and retrograde spanwise vortices respectively) correspond to the head and neck portion of the hairpins. In the vicinity of the prograde vortices, much stronger activities of the ejection and sweep motions were observed in the experiment. Natrajan et al.[10] found that although the shear stress close to the core of prograde vortices is comparably small (5% – 10%), the induced ejection and sweep events contribute significantly to the shear stress in the boundary layer, taking up 30% of the total mean shear.

The hairpin vortex structure can accelerate momentum transportation, thus modifying the momentum distribution in turbulent boundary layer. Instantaneous velocity field can be divided into several zones according to the Probability Density Function (PDF) of the streamwise velocity. Each zone has relative uniform streamwise momentum, referred to as Uniform Momentum Zone (UMZ). A steep velocity gradient appears across the edges of UMZ.[1] Adrian et al.[1] studied the instantaneous velocity field of turbulent boundary layer and found that the formation and distribution of UMZs are closely related to the occurrence of hairpin vortices. They pointed out that the UMZ edges pass through the core of hairpin vortex head. de Silva et al.[11,12] compared the distribution and statistical properties of UMZ for the smooth surface turbulent boundary layers at different Reynolds numbers. They found that with the increase of Reynolds number, the average number of UMZs ($\bar{N}_{\mathrm{UMZ}}$) gradually increases, holding a logarithmic relation between the former parameters. Wu and Christensen[13] studied the spatial distribution of spanwise vortices at different Reynolds numbers and showed that the number of spanwise vortices in the turbulent boundary layer increases with increasing Reynolds number. Furthermore, de Silva et al.[11] analyzed the synthetic instantaneous velocity fields that satisfy the attached eddy model proposed by Perry and Marusic,[14] and in this model the "attached eddy" means a set of geometrically similar eddies consisting of a range of length scales with individual scales proportional to the distance at which the eddy is located from the wall. The comparison between the UMZ distribution obtained from Attached Eddy Model (AEM) and results obtained from the PIV measurement yields good agreement,[11] which further proved that the coherent structures are responsible for the distribution of UMZ in turbulent boundary layer.

Previous studies mainly focus on the dynamic behavior and momentum distribution of turbulent boundary layer over smooth surface. However, it is not clear whether surface type will affect the coherent structure and the UMZ characteristics. The surface texture, including riblets, dimples and roughness, has been actively investigated since 1980s due to their viscous drag reduction effect.[15–17] Wang et al.[18] investigated the statistical properties and coherent structures of turbulent boundary layer developed over riblet surface with hydrogen bubble flow visualization and Laser Doppler Velocimetry (LDV). They pointed out that the thickness of viscous sublayer and buffer layer increase over streamwise riblet surface compared with turbulent boundary layer over smooth surface, indicating the drag reduction effect. Bechert et al.[16] conducted extensive investigations on blade-shaped and trapezoidal-groove riblets, and showed the latter as a compromise between optimal drag-reduction performance and practical fabrication and maintenance. They proposed that with a spanwise spacing s^+ of 15–20 and height to span ratio (h/s) of 0.5–0.8, the streamwise riblets can lead to the maximum drag reduction of 10%.[16,19] The drag reduction is proportional to the riblet size within a range of s^+ and h^+.[16] However, further size increase leads to the breakdown of proportionality, and even drag increase.[20] A recent study on the drag-reduction of the riblets performed by García-Mayoral and Jiménez[21] showed that the breakdown of the proportionality can be better characterized by the riblet cross-section area instead of riblet spacing, and it is associated with the appearance of quasi-two-dimensional spanwise vortices in buffer layer. They proposed a simplified stability model to approximately account for the drag-reduction change with the riblet cross-section area.

Two main mechanisms have been proposed to explain the physical mechanism behind the drag reduction effect of riblet surfaces. One suggests that the riblets suppress the momentum transport along spanwise direction, thus reducing the spanwise component of velocity fluctuations.[22] The other claims that the riblets with certain spanwise spacing have a 'lift-up' effect on streamwise vortices, which reduces the momentum transport along the wall-normal direction in the near wall region.[23] Besides, Bacher and Smith[24] proposed the second vortex group mechanism by considering the interaction of the counter-rotating longitudinal vortices with small vortices created by them near the riblets peak, arguing that the secondary vortices would weaken the longitudinal vortices as well as retain the low-speed fluid within the riblets.

To further understand the drag reduction mechanism over directional riblet surface, Nugroho et al.[25] analyzed the effect of convergent and divergent riblets pattern on turbulent boundary layers using hot-wire anemometry. Results showed that the riblets introduce spanwise modification to the boundary layer, redistributing the large-scale coherent structures. The pre-multiplied energy spectra suggested that the energy magnitude of the coherent structures increases over convergent riblets while decreases over divergent riblets, indicating an evident directional influence. Compared to the streamwise riblets, the drag-reduction effect of the inclined riblets can be weakened by the increase of the yaw angle.[26] However, the spatial temporal distribution of the large-scale coherent structures cannot be directly obtained from the pointwise measurement. More detailed diagnostic techniques are needed.

The present study uses particle image velocimetry to investigate the effect of streamwise riblet surface on the distribution of coherent structures in turbulent boundary layer. The distribution of uniform momentum zone is discussed and compared with smooth surface boundary layer, yielding the correlation between coherent structures and momentum distribution. The experimental setup and facilities are detailed in Section 2. The time-averaged and instantaneous properties of the turbulent boundary layer over both smooth and riblet surfaces are discussed in Section 3. The effect of streamwise riblet surface on the distribution of coherent structures and the relation with uniform momentum zones are analyzed. The Reynolds number influence on momentum distribution is further addressed.

2. Experimental setup test facilities

The experiment was performed in the closed-loop low-speed water tunnel of Beihang University (BUAA), with a test

section of 3000 mm × 600 mm × 600 mm (length × width × height). The freestream velocity U_∞ of the flow is 192 mm/s, with a turbulence level controlled below 1%.

A flat plate was mounted on the bottom wall of the water tunnel. The length, span and thickness of the plat are 2400 mm, 600 mm and 10 mm respectively. The front end of the flat plate has a sloping surface with length-to-height ratio of 8:1, which was used to avoid leading edge separation. Two types of plate surfaces, including smooth and streamwise riblet surface, were compared in this experiment. The experimental setup is shown in Fig. 1(a). The riblet has a trapezoidal-shaped cross-section with a height (h) of 1.5 mm, a spanwise spacing (s) of 1.932 mm and a vertex angle of 60°, as shown in Fig. 1(b). The non-dimensional spacing s^+ and height h^+ of the riblet are 16.3 and 12.6, within the range of maximum drag reduction.[16] The bottom plateau of 0.2 mm is observed due to limited machining precision. In order to obtain fully developed turbulent boundary layer before the measurement domain, cylindrical tripwires of 3 mm height were placed at the leading edge of the plate to trip early transition for both smooth and riblet surface ($x = 0$). The measurement domain starts from 1800 mm downstream of the tripwire location where the turbulent boundary layer has been fully developed. The measurement Field Of View (FOV) is 95 mm × 95 mm. The boundary layer thickness of the tunnel side wall at the center location of the FOV is less than 35 mm, which is almost one order magnitude smaller than the half-width (300 mm) of the tunnel, and therefore the side wall effect on the flow can be neglected. The coordinate axes x, y and z are designated as streamwise, wall-normal and spanwise direction, respectively. The corresponding velocities are represented by u, v and w. The origin of the coordinate system locates at the start of the measurement domain in streamwise direction and the smooth wall location in wall-normal direction, as shown in Fig. 1.

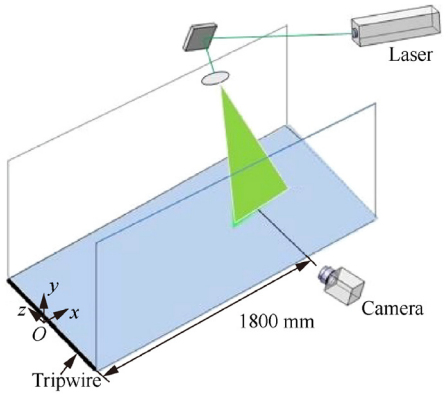

(a) Experimental setup

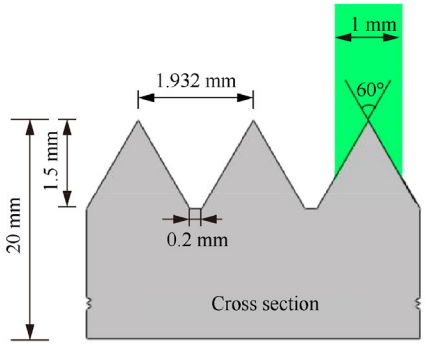

(b) Cross-section of riblets
(Green shadow indicates laser illuminated area)

Fig. 1 Schematic diagram of experimental setup and riblet surface.

Two-dimensional particle image velocimetry (2D-PIV) was used in the experiment to measure the instantaneous velocity field in the symmetric plane of the plates. The measurement plane (x-y plane) was illuminated by a Vlite-Hi-30 K solid-state laser (32 mJ/pulse, 527 nm wavelength, 3 kHz maximum frequency) with a laser thickness of approximately 1 mm. The laser sheet was placed at the peak of trapezoidal-shaped riblet. The fluid was seeded with hollow glass tracer particles with mean diameter of 10 μm and density of 1.05 g/cm^3. The particle images were recorded by a high-speed CMOS camera (2048 pixels × 2048 pixels, 21.7 pixel/mm) with an objective of 90 mm. Table 1 gives an overview of the parameters for the PIV measurement. The sampling frequency of the camera is 300 Hz. The particle displacement in the freestream is about 12 pixels. The particles have an image size of two or three pixels, which avoids the peak locking problem.[27] The velocity field is calculated using Multi-pass Iterative Lucas-Kanade (MILK) algorithm.[28] The final interrogation window is 32 pixels × 32 pixels, with an overlap of 75%. The resultant vector pitch is 0.37 mm. 5456 single particle images were recorded in every sampling period. For each surface condition, five periods were tested. The total sampling time was more than 1.5 min, ensuring statistical convergence.

3. Results and discussion

3.1. Statistical analysis of turbulent boundary layer

For the turbulent boundary layer over smooth plate, the friction velocity (u_τ) can be obtained by the linear fit to the logarithmic region in mean velocity profile.[29] Due to the uncertainty of the wall position caused by the riblet surface, a modification to the logarithmic equation is applied:

$$u^+ = \frac{1}{\kappa}\ln \hat{y}^+ + \mathrm{B} + \Delta u^+ \tag{1}$$

where κ and B are the log-law constants, $\hat{y}$ is defined as the wall-normal distance from the vertex of the riblets plus the roughness offset ($\hat{y} = y + y_v$) and Δu^+ is the velocity offset of the logarithmic profile caused by the riblets. Differentiating Eq. (1) by y yields

Table 1 Parameters for PIV measurement.

Parameter	Symbol	Value
Field of view	FOV	95 mm × 95 mm
Digital image resolution	R	21.7 pixel/mm
Acquisition frequency	f	300 Hz
Number of frames	N	27280
Objective	O	90 mm
Interrogation window	M	32 pixels × 32 pixels, 75% overlap
Vector pitch	P	0.37 mm

$$\frac{\Delta u}{\Delta y} = \frac{u_\tau}{\kappa} \cdot \frac{1}{y + y_v} \tag{2}$$

where the friction velocity (u_τ) and roughness offset (y_v) can be estimated by modified Clauser equation. The time-averaged velocity profiles along smooth and riblet surface are shown in Fig. 2. Compared with the smooth surface, a significant upward shift of the logarithmic region is observed for the riblet surface. This is in agreement with the experimental result of Choi,[30] Bechert et al.[16] and Wang et al.[18] The detailed boundary layer properties are summarized in Table 2, where U_∞ and u_τ are free stream velocity and wall friction velocity, C_f is the wall friction coefficient, δ is the boundary layer thickness, Re_τ is the Reynolds number, and H is the shape factor. The boundary layer thickness over the riblet surface is similar to that of the smooth surface. The smaller friction velocity at the riblet surface indicates a skin friction reduction effect. The effect of riblet surface on velocity fluctuations is also analyzed with non-dimensional root mean square of the streamwise velocity (u^+_{rms}), as shown in Fig. 2(b). Good agreement is found between the smooth surface measurement and the analytical model proposed by Marusic and Kunkel.[31] Over riblet surface, the velocity fluctuations decrease in the near wall region ($y^+ < 60$), reaching comparable level with smooth surface when moving away from the wall. As a result, the effect of riblet surface on velocity fluctuations mainly focuses on the viscous sublayer and buffer layer.

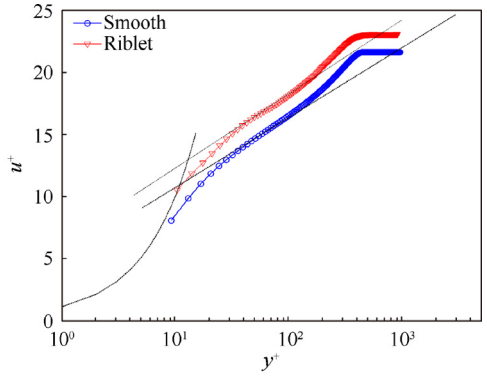

(a) Time-averaged streamwise velocity profile

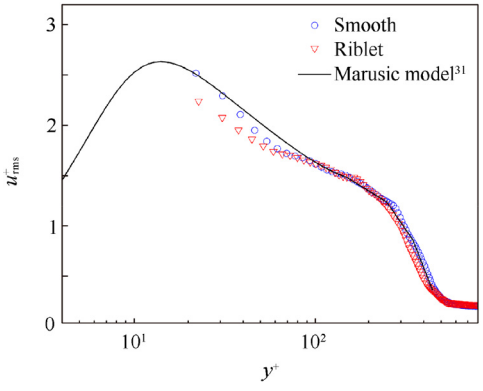

(b) Streamwise velocity fluctuations

Fig. 2 Velocity and velocity fluctuation profiles over smooth and riblet surfaces.

It has been found that the irregular rough surfaces will influence the shear stress within a turbulent boundary layer.[32] Cui et al.[33] and Wu et al.[34] studied the effect of convergent and divergent riblets on turbulent boundary layer and found that the two directional riblet surfaces have opposite effects on Reynolds shear stress. The convergent riblets cause an increased shear stress, while the divergent type leads to shear stress reduction. In the present experiment, the Reynolds shear stress ($-<u'v'>$) normalized by U_∞^2 over the streamwise riblet surface is also compared with that of smooth surface, as shown in Fig. 3. The shear stress over both surfaces reaches the maximum very close to the wall, followed by a rapid decrease when moving upward. Compared to the smooth surface, the Reynolds shear stress of the riblet surface is significantly reduced. When using y^+ as the wall-normal coordinate, Fig. 3 shows that the Reynolds shear stress of riblet surface is smaller than the smooth surface over the entire boundary layer. The change of the shear stress relates to the change of skin friction, which further reveals the drag reduction effect of the streamwise riblet surface.

3.2. Vortex structure

3.2.1. Vortex identification method

In order to detect spanwise vortices in the turbulent boundary layer over smooth and riblet surface, Galilean decomposition and swirling strength criterion are applied and compared by Cui et al.[33] The instantaneous vector field after Galilean decomposition is shown in Fig. 4(a). Fig. 4(b) shows the prograde and retrograde vortices (colored blue and red) in boundary layer. The convective velocity U_c of the spanwise vortices

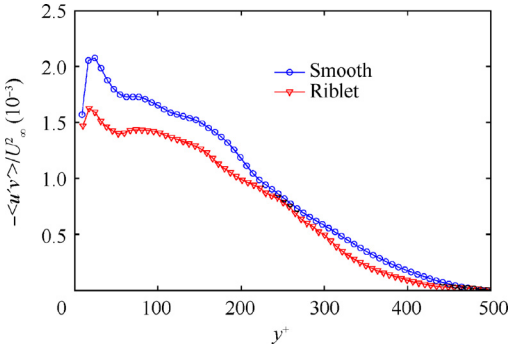

Fig. 3 Reynolds shear stress over smooth and riblet surfaces.

Table 2 Turbulent boundary layer properties over smooth and riblet surface.

Parameter	U_∞ (mm/s)	u_τ (mm/s)	C_f (10^3)	δ (mm)	s^+	h^+	Re_τ	H
Smooth	192.3	9.3	4.67	59.6			510	1.34
Riblet	192.2	8.9	4.29	59.0	16.3	12.6	490	1.32

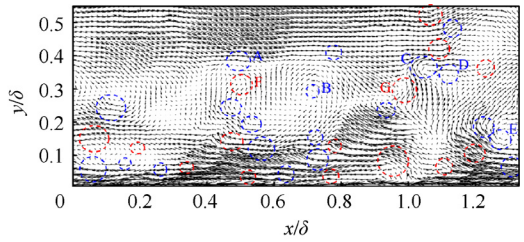

(a) Instantaneous vector field after Galilean decomposition (convective velocity U_c=0.87U_∞)

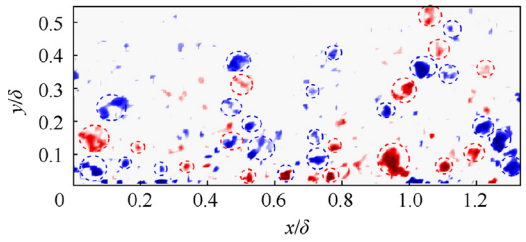

(b) Λ_{ci} field

Fig. 4 Cross-sections of vortex structures.

$0.87U_\infty$ is subtracted from the velocity field. The large-scale vortex structures (A–G) can be clearly identified.

The swirling strength is calculated as follows:

$$\Lambda_{ci} = \lambda_{ci}\frac{\omega_z}{|\omega_z|} \tag{3}$$

where ω_z denotes the vorticity, λ_{ci} and Λ_{ci} are swirling strength and swirling strength normalized by the vorticity. The rotating direction is determined by the sign of the local spanwise vorticity, as shown in Fig. 4(b). Compared to Galilean decomposition, vortices with different convection velocities can be easily recognized. As a result, swirling strength is used as the main vortex identification method in the following analysis.

According to the analysis of Zhou et al.,[35] Natrajan et al.[10] and Lee and Choi,[36] the prograde and retrograde vortices correspond to the head and neck portion of the hairpin vortices. Instead of good spanwise symmetry, the hairpin vortices usually appear as 'cane' shape, and therefore the spanwise vortices do not appear in pairs in single cross-plane. In the present experiment, the prograde vortices are more populated and have higher vorticity than retrograde ones, as shown in Fig. 4(b). Strong ejection (Q2) and sweep (Q4) events are induced in the upstream (bottom) and downstream (top) of prograde vortices (see Fig. 4(a) *C*, *E*), leading to the formation of strong shear layer in the vicinity, which agrees with the analysis of Adrian,[2] Kang et al.[37] and Kim et al.[38] The former studies proposed that the skin friction is mostly contributed by the hairpin vortices. In the following analysis, the distribution of the hairpin vortex structures is represented by the spanwise prograde vortices, referred to as hairpin head. The effect of streamwise riblet surface on the distribution of hairpin heads and drag reduction will be further discussed.

3.2.2. Distribution of prograde vortices

In order to understand the effect of streamwise riblet surface on the distribution of prograde vortices, it is essential to accurately detect the vortex structures. Two major parameters have to be considered, namely the critical swirling strength (Λ_{ci}) and the vortex size. Following Wu and Christensen[13] and Cui et al.,[33] the vortex structure is considered when $\Lambda_{ci}(x,y)$ is smaller than $-1.5\Lambda_{ci}^{rms}(y)$. Furthermore, each vortex needs to have the spatial distribution larger than 5 vector grids in both streamwise and wall-normal directions. The inner scale is larger than 20y*, where $y^* = \nu/u_\tau$, similar to the threshold used by Wu and Christensen.[13]

The number of prograde vortices over both smooth and riblet surfaces along wall-normal direction is shown in Fig. 5. $\Pi_p(y)$ is the number of prograde vortices at different wall-normal positions. The wall-normal positions of the vortices are decided by the vortex core. The wall-normal axis is non-dimensionalized by boundary layer thickness and in wall unit, as shown in Fig. 5(a), (b) respectively. The number of prograde vortices increases steeply when moving from the wall until $y/\delta = 0.12$ ($y^+ = 60$), followed by a slight decrease when further developing towards Turbulent/Non-Turbulent Interface (TNTI). The location of the largest number of vortices corresponds to the logarithmic region. Similar scenario on hairpin vortex distribution inside turbulent boundary layer was also observed by Adrian.[2] Over the entire boundary layer, the number of prograde vortices is smaller over riblet surface than that of smooth surface. The difference is more evident when using y^+ as the wall-normal height, indicating the impact of surface type on the vortex structures.[33] As surface skin friction highly relates to the hairpin vortices in the boundary layer,[38] the decrease number of hairpins yields lower friction velocity and skin friction, further proving the drag reduction effect of the streamwise riblet surface.

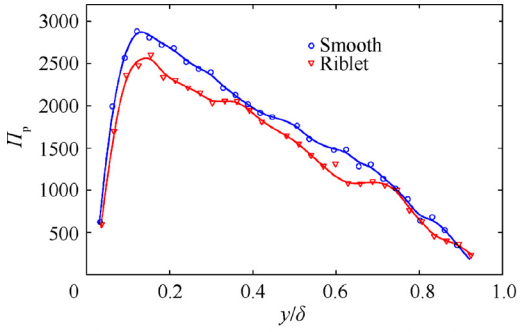

(a) Number of prograde vortices normalized by δ

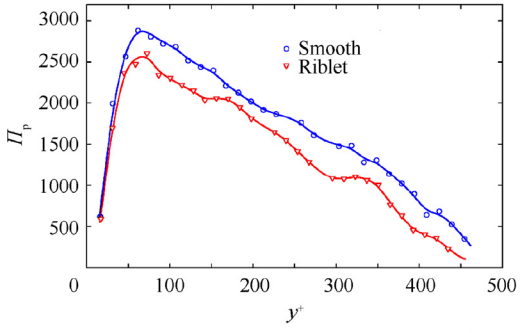

(b) Number of prograde vortices normalized by wall unit

Fig. 5 Number of prograde vortices along wall-normal direction.

3.2.3. Two-point correlation

In turbulent boundary layer, it has been suggested that the dominant coherent structure is the multi-scale hairpin vortex packets.[2] As discussed in Section 3.2.2, the streamwise riblet surface influences the number of hairpin vortices in turbulent boundary layer. The distribution of the hairpin vortices can be further characterized using two-point velocity fluctuation correlation, as the streamwise extent of the correlation coefficient relates to the distribution of hairpin packets at a certain height inside the boundary layer.[39] The quantitative analysis of the coherent structures is performed using two-point correlation as

$$\rho_{ij}(x_{\mathrm{r}}, y; y_{\mathrm{ref}}) = \frac{\left\langle u_i'(x, y_{\mathrm{ref}}, t) u_j'(x + x_{\mathrm{r}}, y, t) \right\rangle}{\| u_i'(x, y_{\mathrm{ref}}, t) \| \| u_j'(x + x_{\mathrm{r}}, y, t) \|} \tag{4}$$

where y_{ref} is the reference wall-normal location, x_{r} is the distance between two correlated points, and $\langle \cdot \rangle$ and $\| \cdot \|$ represent the inner product and 2-norm of a matrix respectively.

The cross-plane contours of two-point velocity fluctuation correlation coefficient ρ_{uu} for smooth and streamwise riblet surface boundary layer are shown in Fig. 6, r_x is the distance between the correlated points and δ_s is the boundary layer thickness of smooth surface. The reference wall-normal location is 0.2δ, which is close to the location of the largest number of hairpin vortices. The correlation coefficient ρ_{uu} has an inclination angle of 10.5° over both surfaces, close to the result by Christensen and Adrian.[40] Wu and Christensen[32] found that the distribution of the two-point correlation coefficient is similar for smooth and rough surfaces. Similar pattern of ρ_{uu} is also found between smooth and riblet surface. The streamwise extent of ρ_{uu} for the riblet surface is smaller than smooth surface type.

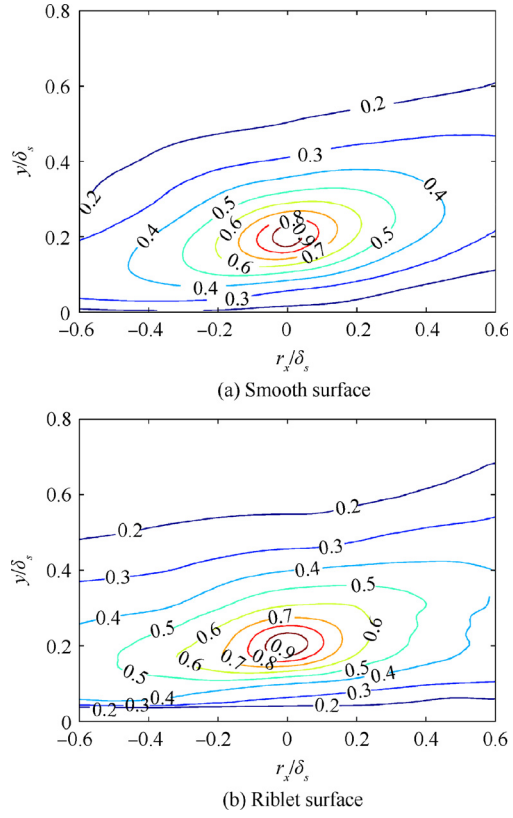

(a) Smooth surface

(b) Riblet surface

Fig. 6 Contour of two-point correlation coefficient ρ_{uu} of streamwise velocity fluctuation.

Quantitative characterization of the streamwise extent (L_x) of ρ_{uu} is performed. According to Christensen and Wu,[41] the streamwise extent (L_x) at $y_{\mathrm{ref}} = 0.2$ is defined as two times the streamwise distance between the correlation level of 0.5 and the correlation peak, shown as $L_x = 2r_x|\rho_{uu} = 0.5$ in Fig. 7. L_x is 12% smaller over riblet surface than smooth surface. Marusic[39] found that the number and distribution of hairpin vortices have a positive correlation with L_x. As a result, the smaller L_x over riblet surface agrees with the decreased number of prograde vortices (hairpin heads) estimated in Section 3.2.2. Similarly, Cui et al.[33] also found that for the riblet surface type of convergent and divergent direction, the number of prograde vortices increases with the increase of the streamwise extent, in accordance with present result. The variation of L_x along wall-normal direction is provided in Fig. 8. The increase of wall-normal distance from the wall leads to the growth of L_x until $y/\delta = 0.3$, reaching a plateau further upward.

3.3. Effect of streamwise riblet surface on uniform momentum zones

3.3.1. UMZ detection and characterization

de Silva et al.[11] made a statistical analysis of the instantaneous velocity field measured by two-dimensional PIV using the probability density function. The characteristics of the momentum zone of turbulent boundary layer at different Reynolds numbers were obtained. The peak value of PDF for streamwise velocity is defined as the modal velocity. The

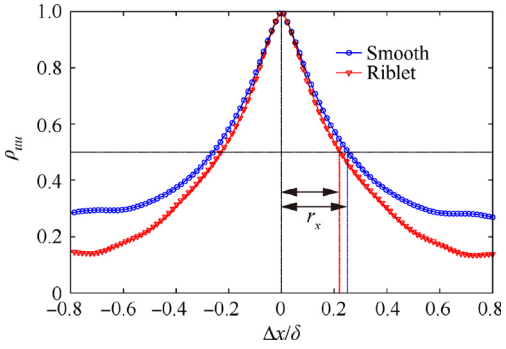

Fig. 7 Streamwise variation of ρ_{uu}.

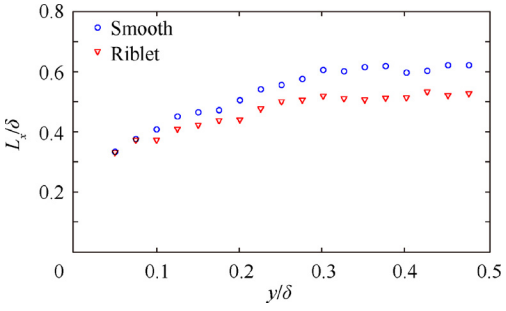

Fig. 8 Wall-normal variation of ρ_{uu}.

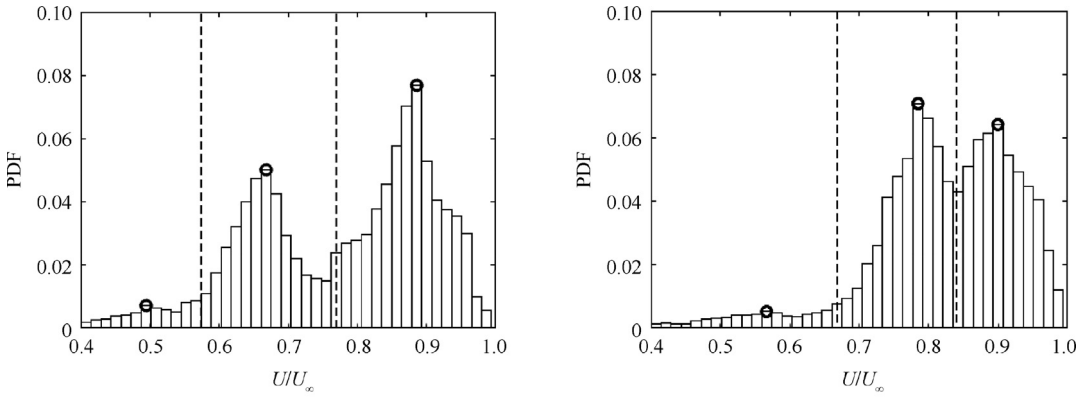

(a) PDF of u over smooth surface (b) PDF of u over riblet surface

Fig. 9 PDF of instantaneous streamwise velocity u.

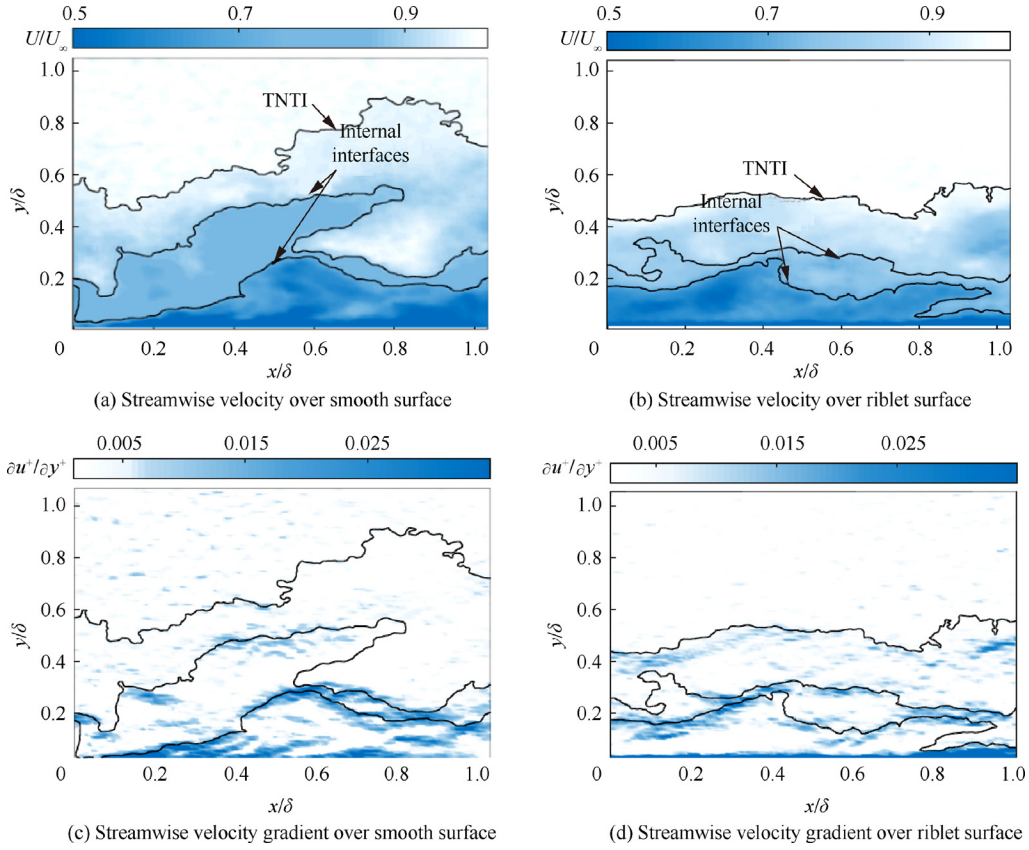

(a) Streamwise velocity over smooth surface (b) Streamwise velocity over riblet surface

(c) Streamwise velocity gradient over smooth surface (d) Streamwise velocity gradient over riblet surface

Fig. 10 x-y contour of streamwise velocity and streamwise velocity gradient.

boundary velocity of a UMZ is defined as the average of two neighboring modal velocities. The boundary between the region of maximum momentum and the non-turbulence region is known as TNTI. The TNTI is determined based on kinetic energy of 0.2 as used by Chauhan et al.[42] de Silva et al.[11] compared the PDF of the streamwise velocity within different streamwise range (from 0.2δ to 2δ) and found that the influence of domain length on the UMZ edge is negligible. Therefore, the steamwise velocity field within TNTI over the entire streamwise measurement range is considered in present work. From the previous analysis, the riblet surface influences the distribution of time-averaged velocity and velocity fluctuations.[18,25] It is still questionable if the overall distribution of the uniform momentum zones will be changed.

The PDF of instantaneous streamwise velocity over both smooth and streamwise riblet surface is shown in Fig. 9. The modal velocity of every UMZ is highlighted by hollow circle (○). The UMZ edges between adjacent zones are shown by dash lines. The corresponding instantaneous streamwise velocity fields are shown in Fig. 10(a) and (b), superimposed by the UMZ edges (black lines). Evident streamwise velocity variation can be found between different UMZs. Large streamwise

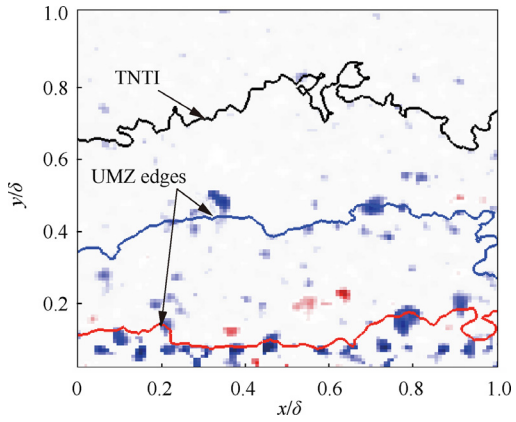

Fig. 11 Λ_{ci} field and UMZ edges.

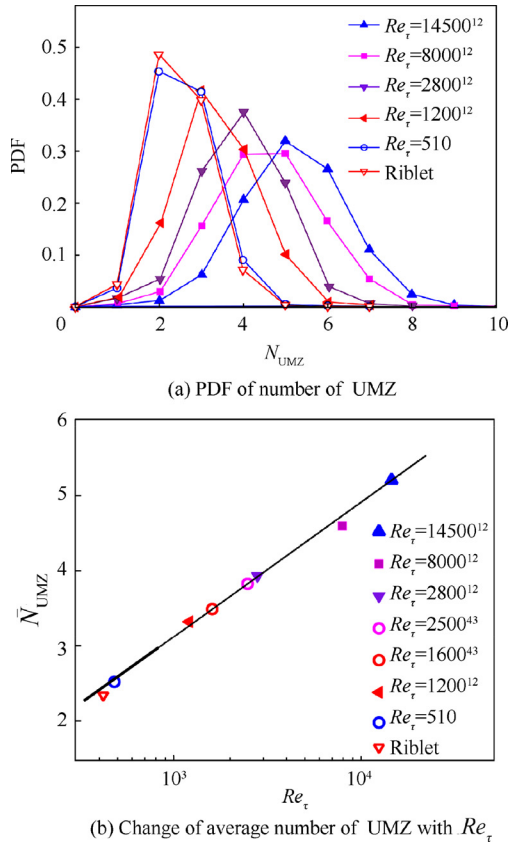

(a) PDF of number of UMZ

(b) Change of average number of UMZ with Re_τ

Fig. 12 Change of UMZ with Reynolds number. Experimental data[12] with Re_τ = 14500(▲), 8000(■), 2800(▼), 1200(◀); DNS data[43] with Re_τ = 2500(○), 1600(○); Present data for smooth(○) and riblet surface(▽).

velocity gradient along wall-normal direction dU/dy occurs at the UMZ edges, as shown in Fig. 10(c) and (d), indicating the prevalence of prograde vortices. de Silva et al.[11] proposed that the formation of UMZ is closely related to the evolution and induction effect of hairpin vortex packets in the turbulent boundary layer. The large velocity gradient at the UMZ edge corresponds to the large spanwise vorticity, where hairpin vortices develop from. Adrian et al.[1] found that the UMZ edges pass through the core of hairpin heads, indicating the connection between UMZ and the distribution of coherent structures in the turbulent boundary layer, which can also be shown in Fig. 11.

3.3.2. *Effect of Reynolds number on UMZ*

In the turbulent boundary layer, the number and scale of the coherent structures are significantly influenced by Reynolds number. As the distribution of UMZ is related to the hairpin vortex packets, the change of the Reynolds number will also influence the UMZ edge location and UMZ characteristics. de Silva et al.[11] studied the variation of the number of UMZ over the smooth surface turbulent boundary layer from medium to high Reynolds numbers. They pointed out that as the Reynolds number increases, the number of UMZ (N_{UMZ}) gradually increases. The average number of UMZ ($\bar{N}_{UMZ}$) follows a logarithmic relationship with Reynolds number. The PDF of the number of UMZs at different Re_τ is analyzed, as shown in Fig. 12(a). The experimental results over smooth surface at medium to high Re_τ (Re_τ = 1400, 2800, 8000, 14500) of de Silva et al.[11] are compared, and the numerical results of Sillero et al.[43] at Re_τ = 1600 and 2500 are also included. In smooth surface boundary layer, the PDF of the number of UMZs shifts to the right with the increase of Reynolds number, indicating a positive correlation. The average number of UMZs of both smooth and riblet surface at different Reynolds numbers are summarized in Table 3. The change of $\bar{N}_{UMZ}$ with Re_τ is plotted in Fig. 12(b). Linear least-square fit is performed and shown as the black-dash line, yielding a logarithmic correlation. By further extending the linear fit to the lower Re_τ range (see the thick line), both smooth and riblet surface conditions of the current experiment fall on the linear fitting. It is conjectured that the number of UMZ is proportional to $\ln(Re_\tau)$, irrespective of the surface type.

4. Conclusions

In this paper, the effect of streamwise riblet surface on the development of turbulent boundary layer is investigated by the two-dimensional particle image velocimetry. Comparison has been made with smooth surface type, focusing on the influence of the streamwise riblet surface on turbulent statistics and coherent structures inside turbulent boundary layer. The results are as follows:

Table 3 Average number of UMZ at different Re_τ.

Re_τ	490	510	1200	1600	2500	2800	8000	14500
$\bar{N}_{UMZ}$	2.51	2.59	3.33	3.49	3.83	3.93	4.59	5.20

1) Compared to the smooth surface, the buffler layer and logarithmic region of time-averaged velocity profile over the streamwie riblet surface show an evident upward shift, along with a slight decrease of the level of turbulent fluctuations. The upward shift of the buffer layer results in the smaller shear stress over streamwise riblet surface and therefore the drag would be reduced.
2) For both surfaces, the number of prograde vortices increases steeply when moving from the wall until the logarithmic region, followed by a slight decrease when further developing towards turbulent/non-turbulent interface. Compared to smooth surface, the amount of prograde vortices is smaller over the streamwise riblet surface. The correspondence decrease of streamwise length scale of the two-point correlation coefficient indicates the reduction of the streamwise scale of the coherent structure. The reduced number of hairpin vortices also modifies the momentum partition in the turbulent boundary layer, yielding fewer UMZs. The number of UMZ holds a logarithmic relationship with Reynolds number over smooth surface. The relation is still valid over streamwise riblet surface at lower Reynolds number.

Acknowledgement

This work was supported by the National Natural Science Foundation of China (Nos. 11721202 and 11672020).

References

1. Adrian RJ, Meinhart CD, Tomkins CD. Vortex organization in the outer region of the turbulent boundary layer. *J Fluid Mech* 2000;**422**:1–54.
2. Adrian RJ. Hairpin vortex organization in wall turbulence. *Phys Fluids* 2007;**19**(4):041301.
3. Head MR, Bandyopadhyay P. New aspects of turbulent boundary-layer structure. *J Fluid Mech* 1981;**107**:297–338.
4. Smith CR, Walker JDA, Haidari AH. On the dynamics of near-wall turbulence. *Phil Trans R Soc Lond A* 1991;**336**(1641):131–75.
5. Tomkins CD, Adrian RJ. Spanwise structure and scale growth in turbulent boundary layers. *J Fluid Mech* 2003;**490**:37–74.
6. Deng SC, Pan C, Wang JJ, He GS. On the spatial organization of hairpin packets in a turbulent boundary layer at low-to-moderate Reynolds number. *J Fluid Mech* 2018;**844**:635–68.
7. Ganapathisubramani B, Longmire EK, Marusic I. Characteristics of vortex packets in turbulent boundary layers. *J Fluid Mech* 2003;**478**:35–46.
8. Robinson SK. Coherent motions in the turbulent boundary layer. *Annu Rev Fluid Mech* 1991;**23**(1):601–39.
9. Lee CB, Li R. Dominant structure for turbulent production in a transitional boundary layer. *J Turbul* 2007;**8**(55):N55.
10. Natrajan VK, Wu Y, Christensen KT. Spatial signatures of retrograde spanwise vortices in wall turbulence. *J Fluid Mech* 2007;**574**:155–67.
11. de Silva CM, Hutchins N, Marusic I. Uniform momentum zones in turbulent boundary layers. *J Fluid Mech* 2016;**786**:309–31.
12. de Silva CM, Philip J, Hutchins N. Interfaces of uniform momentum zones in turbulent boundary layers. *J Fluid Mech* 2017;**820**:451–78.
13. Wu Y, Christensen KT. Population trends of spanwise vortices in wall turbulence. *J Fluid Mech* 2006;**568**:55–76.
14. Perry AE, Marusic I. A wall-wake model for the turbulence structure of boundary layers. Part 1. Extension of the attached eddy hypothesis. *J Fluid Mech* 1995;**298**:361–88.
15. Walsh MJ. Riblets as a viscous drag reduction technique. *AIAA J* 1983;**21**(4):485–6.
16. Bechert DW, Bruse M, Hage W. Experiments on drag-reducing surfaces and their optimization with an adjustable geometry. *J Fluid Mech* 1997;**338**:59–87.
17. Wang JJ. Reviews and prospects in turbulent drag reduction over riblets surface. *J Beijing Univ Aeronaut Astronaut* 1998;**24**(1):31–4 [Chinese].
18. Wang JJ, Lan SL, Chen G. Experimental study on the turbulent boundary layer flow over riblets surface. *Fluid Dyn Res* 2000;**27**(4):217–29 [Chinese].
19. Martin S, Bhushan B. Fluid flow analysis of a shark-inspired microstructure. *J Fluid Mech* 2014;**756**:5–29.
20. Choi H, Moin P, Kim J. Direct numerical simulation of turbulent flow over riblets. *J Fluid Mech* 1993;**255**:503–39.
21. García-Mayoral R, Jiménez J. Drag reduction by riblets. *Phil Trans R Soc Lond A* 1940;**2011**(369):1412–27.
22. Lee SJ, Lee SH. Flow field analysis of a turbulent boundary layer over a riblet surface. *Exp Fluids* 2001;**30**(2):153–66.
23. Goldstein D, Handler R, Sirovich L. Direct numerical simulation of turbulent flow over a modeled riblet covered surface. *J Fluid Mech* 1995;**302**:333–76.
24. Bacher E, Smith C. A combined visualization-anemometry study of the turbulent drag reducing mechanisms of triangular micro-groove surface modifications. Reston: AIAA; 1985. Report No.: AIAA-1985-0548.
25. Nugroho B, Hutchins N, Monty JP. Large-scale spanwise periodicity in a turbulent boundary layer induced by highly ordered and directional surface roughness. *Int J Heat Fluid Flow* 2013;**41**:90–102.
26. Hage W, Bechert DW, Bruse M. *Yaw angle effects on optimized riblets*. Berlin: Springer; 2001. p. 278–85.
27. Christensen KT. The influence of peak-locking errors on turbulence statistics computed from PIV ensembles. *Exp Fluids* 2004;**36**(3):484–97.
28. Champagnat F, Plyer A, Le Besnerais G. Fast and accurate PIV computation using highly parallel iterative correlation maximization. *Exp Fluids* 2011;**50**(4):1169.
29. Clauser FH. Turbulent boundary layers in adverse pressure gradients. *J Aeronaut Sci* 1954;**21**(2):91–108.
30. Choi KS. Near-wall structure of a turbulent boundary layer with riblets. *J Fluid Mech* 1989;**208**:417–58.
31. Marusic I, Kunkel GJ. Streamwise turbulence intensity formulation for flat-plate boundary layers. *Phys Fluids* 2003;**15**(8):2461–4.
32. Wu Y, Christensen KT. Spatial structure of a turbulent boundary layer with irregular surface roughness. *J Fluid Mech* 2010;**655**:380–418.
33. Cui GY, Pan C, Gao Q, Rinoshika A, Wang JJ. Flow structure in turbulent boundary layer over directional riblets surfaces. *Acta Mech Sin* 2017;**49**(6):1201–12 [Chinese].
34. Wu D, Wang JJ, Cui GY, Pan C. Effects of surface shapes on properties of turbulent/non-turbulent interface in turbulent boundary layers. *Sci China Technol Sci* 2018 (2018-12-12) [2019-04-10] http://engine.scichina.com/doi/10.1007/s11431-018-9434-5.
35. Zhou J, Adrian RJ, Balachandar S. Mechanisms for generating coherent packets of hairpin vortices in channel flow. *J Fluid Mech* 1999;**387**:353–96.
36. Lee SJ, Choi YS. Decrement of spanwise vortices by a drag-reducing riblet surface. *J Turbul* 2008;**9**(23):N23.
37. Kang YD, Choi KS, Chun HH. Direct intervention of hairpin structures for turbulent boundary-layer control. *Phys Fluids* 2008;**20**(10):101517.
38. Kim K, Adrian RJ, Balachandar S. Dynamics of hairpin vortices and polymer-induced turbulent drag reduction. *Phys Rev Lett* 2008;**100**(13):134504.
39. Marusic I. On the role of large-scale structures in wall turbulence. *Phys Fluids* 2001;**13**(3):735–43.

40. Christensen KT, Adrian RJ. Statistical evidence of hairpin vortex packets in wall turbulence. *J Fluid Mech* 2001;**431**:433–43.
41. Christensen KT, Wu Y. *Characteristics of vortex organization in the outer layer of wall turbulence*. Begel House Inc.; 2005.
42. Chauhan K, Philip J, de Silva CM. The turbulent/non-turbulent interface and entrainment in a boundary layer. *J Fluid Mech* 2014;**742**:119–51.
43. Sillero JA, Jiménez J, Moser RD. One-point statistics for turbulent wall-bounded flows at Reynolds numbers up to $\delta^+ \approx 2000$. *Phys Fluids* 2013;**25**(10):105102.